

# Fabrication of Large Scale Self-supported WC/Ni(OH)<sub>2</sub> Electrode for High-current-density Hydrogen Evolution<sup>①</sup>

LI Ping-Yu<sup>a, b</sup> HONG Wen-Ting<sup>a</sup> LIU Wei<sup>a②</sup>

<sup>a</sup> (CAS Key Laboratory of Design and Assembly of Functional Nanostructures, and Fujian Provincial Key Laboratory of Nanomaterials, Fujian Institute of Research on the Structure of Matter, Chinese Academy of Sciences, Fuzhou 350002, China)

<sup>b</sup> (University of Chinese Academy of Sciences, Beijing 100049, China)

**ABSTRACT** In the industry, cheap and stable electrocatalysts are eagerly expected for hydrogen evolution reaction (HER) at a high current density. Two-component electrochemical catalysts with integrated multiple interfaces seem to be an expedient strategy to enhance the inherent electronic structure of hybrid electrocatalysts and optimize the catalytic ability. In this work, we report an active tungsten carbide and nickel hydroxide (WC/Ni(OH)<sub>2</sub>) electrocatalyst seamlessly synthesized on the substrate of W foil. Ni(OH)<sub>2</sub> trends to adsorb OH<sub>ad</sub> and WC can effectively adsorb H<sub>ad</sub>. Prompted by the synergistic effect, the ability of the catalyst manifests an effective HER kinetics with an overpotential of 475 mV (vs. RHE) at a high current density of 1000 mA/cm<sup>2</sup> in 1 M KOH. Moreover, due to its self-supported construction, the catalyst presents reliable long-term stability with no obvious active property loss after 8000 cycles and 50 hours of operation in an alkaline solution.

**Keywords:** hydrogen evolution reaction, tungsten carbide, nickel hydroxide, high current density;

**DOI:** 10.14102/j.cnki.0254-5861.2011-3168

## 1 INTRODUCTION

Due to the accelerating consumption of fossil fuels, environmental contamination, and global warming, the development of clean and renewable resources has become an exceedingly urgent concern to be solved<sup>[1]</sup>. Hydrogen (H<sub>2</sub>), as a highly attractive and low-contamination resource with immense energy density, has been proposed as an encouraging alternative<sup>[2]</sup>. In order to produce hydrogen efficiently and cyclically, water splitting with an electrochemical approach is an efficient route to synthesize hydrogen production<sup>[3]</sup>. Up to now, noble metals, such as platinum (Pt), have been utilized as electrocatalysts in hydrogen evolution reaction (HER) to highly improve the reaction efficiency because of its approximately zero overpotential<sup>[4]</sup>. At present, Pt is used as an electrode material in alkaline solution in the industry. However, large scale applications are still restricted because of their high cost and low reserves on

the earth<sup>[5]</sup>. As a result, replacing noble materials with economical and durable catalysts is an urgent issue.

In recent decades, more and more transition metal-based materials (phosphides<sup>[6]</sup>, sulfides<sup>[7]</sup>, carbides<sup>[8]</sup>, etc.) are put into use as electrocatalysts in HER, instead of noble metal materials. It is a feasible solution to combine the two components to optimize the hydrogen adsorption and desorption capacity<sup>[9]</sup>. The synergistic effects can be also induced by hybridizing different components including the regulation of electronic structure, the arrangement of the atom, and the stabilization of interface, which can advance the catalytic capability of HER<sup>[10, 11]</sup>. In particular, the ample interfaces between different components play an important role in transporting surface matter like electrons and adsorbents<sup>[10]</sup>. Ma's group synthesized an inlaid ultrathin MoS<sub>2</sub>/graphene nanosheets by a thermal process, manifesting a prompt hydrogen evolution performance with the overpotential of 110 mV at a current density of 10 mA/cm<sup>2</sup> and a small Tafel slope

Received 2 March 2021; accepted 7 April 2021

① This research was supported by the National Natural Science Foundation of China (Nos. 61674152 and 51902309)

② Corresponding author. E-mail: liuw@fjirsm.ac.cn

of 67.4 mV/dec<sup>[12]</sup>. Shi's group reported a W<sub>2</sub>C/WP catalyst via a one-step process with 83 mV overpotential at a current density of 10 mA/cm<sup>2</sup><sup>[13]</sup>. Moreover, the current density required for industrial alkaline electrolyzers and membranes from proton exchange is normally higher than 500 and 1000 mA/cm<sup>2</sup><sup>[14]</sup>. Zhang's group reported two-dimensional MoS<sub>2</sub>/Mo<sub>2</sub>C catalysts with an overpotential of 412 mV at a high current density of 1000 mA/cm<sup>2</sup><sup>[14]</sup>. Chen group synthesized a MoB<sub>2</sub> that delivers a larger current density and stability of 10 hours of operation<sup>[15]</sup>. However, the cost and the electrochemical, as well as the mechanical stability, need to be further improved.

Herein, we report a promising and highly active WC/Ni(OH)<sub>2</sub> electrode with high current density, which can be synthesized by a simple method for a large scale (Fig. 1). This method supplies a seamless electrical contact between WC/Ni(OH)<sub>2</sub> and W substrate, thus diminishing the loss of voltage and improving the HER performance of WC/Ni(OH)<sub>2</sub> electrode (Fig. 1a)<sup>[16]</sup>. The deposition of Ni(OH)<sub>2</sub> nanoparticles provides more active sites (Fig. 1b)<sup>[17]</sup>. Furthermore, WC is endowed with the characteristic similar to Pt for its broadened *d*-orbital of W after hybridizing with *s*- and *p*-orbitals of carbon<sup>[18]</sup>. Therefore, the capability of hydrogen adsorption for WC is neither strong nor weak<sup>[19]</sup>. Besides, Ni(OH)<sub>2</sub> improves the dissociation of water and binds OH<sub>ad</sub> appropriately (Fig. 1b)<sup>[19, 20]</sup>. Under the synergy of Ni(OH)<sub>2</sub> and WC, the WC/Ni(OH)<sub>2</sub> nanostructure exhibits an extremely higher performance compared with the single WC catalyst. The WC/Ni(OH)<sub>2</sub> has a small Tafel slope of 47.5 mV/dec, a high current density of 1000 mA/cm<sup>2</sup> at 475 mV versus the reversible hydrogen electrode (vs. RHE), and good stability for 50 h at the current density of 500 mA/cm<sup>2</sup> because of its self-supported structure.

## 2 EXPERIMENTAL

### 2.1 Materials

All chemical reagents are commercially available and can be used directly without further purification.

### 2.2 Synthesis of the WO<sub>3</sub> foils

The tungsten (W) foils were polished with abrasive paper to remove the oxide layer on the surface, and the treated W foils were soaked in acetone at 80 °C for 30 minutes. After that, the W foils were taken out and washed by an ultrasonic cleaner (GT Sonic) for 30 minutes with deionized water and ethanol.

The W foils were obtained after drying. The processed W foils were put on a porcelain boat by a chemical vapor deposition (CVD) process in the atmosphere of 80% air and 20% argon (Ar) at 800 °C for 30 minutes with a heating rate of 20 °C/min, with the as-obtained sample to be WO<sub>3</sub>.

### 2.3 Synthesis of the WC foils

The as-obtained WO<sub>3</sub> foils were grown in the tube furnace. The temperature of the furnace was increased to 900 °C followed by flowing with an Ar and H<sub>2</sub> mixture (20:20 sccm) for 30 minutes and adding CH<sub>4</sub> flow (40 sccm) into the carbonization chamber for carbonization for 60 minutes. The heating of the chamber of carbonization was 900 °C at a stable rate of 30 °C/min. After a bunch of reactions above, the furnace was cooled down to room temperature naturally.

### 2.4 Synthesis of WC/Ni(OH)<sub>2</sub>

Before electrodeposition, the ohmic contact was prepared as follows: Firstly, rinse the WC foils with absolute ethanol and deionized water in turn. Secondly, the electric contact was made by using an alligator clip on the WC foil. The whole surface of WC foil was buried in the solution that consists of 0.1 M NiCl<sub>2</sub>·6H<sub>2</sub>O and 0.1 M H<sub>3</sub>BO<sub>3</sub>. A graphite rod was used as the counter electrode and the reference electrode was mercuric oxide. The electrodeposition process of Ni(OH)<sub>2</sub> was completed at a constant potential of -1.5 V for a certain time (20 s was great in experiments). After that, clean the surface with deionized water and dry it with a hot dryer.

### 2.5 Materials characterization

The investigations of microstructures and morphologies were accomplished by the field-emission scanning electron microscopy (Zeiss) and high-resolution transmission electron microscopy (HRTEM) (JEOL, JEM-3000F FEGTEM, 300 kV). The examination of the WC/Ni(OH)<sub>2</sub> formation was finished by Micro-Taman spectroscopy (LabRAM HR Evolution) with a 532 nm laser. XRD analyses were accomplished on the machine Rigaku Ultima IV diffractometer (CuK $\alpha$  radiation,  $\lambda$  = 1.5406 Å) at 40 kV operating voltage and 44 mA operating current. The measurements of XPS were handled on the system of ESCALAB 250Xi (Thermo Fisher) with the source of 100 W AlK $\alpha$  at the incident angle of 45 ° and a size of 100  $\mu$ m spot. The scanning range of binding energy was from 0 to 1200 eV at the step length of 1 eV; high-intensity excitation was supported by AlK $\alpha$  with monochrome X-ray whose energy was 1486.6 eV and the resolution of half maximum of full width was 0.48 eV. Every XPS spectra in 50 meV resolution after calibrating the binding energy of carbon of 284.8 eV were recorded. Gaussian

function was used to get the positions of deconvoluted peak after the correction of nonlinear emission background.

## 2.6 Electrochemical measurements

All measurements of electrochemistry were operated on an electrochemical workstation (CHI 660 e) which includes three standard electrodes configuration at 25 °C. A mercuric oxide electrode and a graphite rod were used as reference electrode and counter electrode, respectively. Every potential of the electrode was transformed to RHE adopting the equation from  $E_{\text{RHE}} = E_{\text{Hg/HgO}} + 0.926 \text{ V}$  in 1 M KOH solution (PH = 14). Refer to the same process, the relationship of the reference electrode (Hg/HgO) and RHE was the equation:  $E_{\text{RHE}} = E_{\text{Hg/HgO}} + 0.983 \text{ V}$  in 10 M KOH solution. Ahead of recording the data, cyclic voltammetry was used to prescan the electrodes for 20 cycles from  $-0.9$  to  $-1.8 \text{ V}$  versus RHE in order to make sure solid CV curves occur. After that, the data of polarization curve about linear sweep voltammetry were collected from the range of  $-0.9$  to  $-1.8 \text{ V}$  with the scan speed of  $5 \text{ mV/s}$  without iR correction. Replotting the polarization curves according to the Tafel equation ( $\eta = b \log(j) + a$ ) can acquire the Tafel plot. Fitting the Tafel plot linear sections can determine the Tafel slope. Measure the material electrochemical stability by adopting the method of cyclic voltammetry at the sweep rate of  $500 \text{ mV/s}$  from  $-0.9 \text{ V}$  to  $-1.8 \text{ V}$  vs. RHE and the method of Amperometric  $i-t$  curve for 50 hours, respectively. IR compensation was not used in the collection of all data.

## 3 RESULTS AND DISCUSSION

### 3.1 Synthesis and characterization

W foil is utilized to synthesize  $\text{WO}_3$ . The synthesis of the  $\text{WO}_3$  layer is on the surface of W foil exposed in the air at  $800 \text{ }^\circ\text{C}$  for 30 minutes. Then, the generated  $\text{WO}_3$  foil is placed in a  $\text{CH}_4/\text{H}_2/\text{Ar}$  atmosphere at  $900 \text{ }^\circ\text{C}$  for 30 minutes to form WC. The synthesis affords the seamless contact between WC and W foil, which reduced the loss of voltage and thus enhanced the HER performance of WC/W. After the fabrication of WC,  $\text{Ni(OH)}_2$  particles are deposited by the method of Amperometric  $i-t$  for 20 s under the potential of  $-1.5 \text{ V}$  in a mixed solution of  $\text{NiCl}_2$  and  $\text{H}_3\text{BO}_3$  (Fig. 1a)<sup>[21]</sup>.

The mechanism of HER for WC/ $\text{Ni(OH)}_2$  catalysts in alkaline solution is presented in Fig. 1b. The step of water dissociation is enhanced by  $\text{Ni(OH)}_2$  and the  $\text{OH}_{\text{ad}}$  adsorption of  $\text{Ni(OH)}_2$  is neither strong nor weak<sup>[20]</sup>. In addition, the capacity adsorbing hydrogen of WC is optimal<sup>[19]</sup>. Therefore, the synergistic integration of WC/ $\text{Ni(OH)}_2$  can highly boost the performance of HER. The morphology of the cross-section of WC (Fig. 1c) shows the strongly tight combination between the WC layer and W foil, indicating that  $\text{WO}_3$  is fully transformed into WC. The ideal interface with a clean and tight connection can improve the charge transport efficiency and boost the HER performance. With this self-supported fabrication process, stable WC/ $\text{Ni(OH)}_2$  hybrid structures on large scale can be prepared on W substrate. The as-grown WC nanostructure synthesized in the laboratory can reach the size of A4 paper (Fig. 1d).

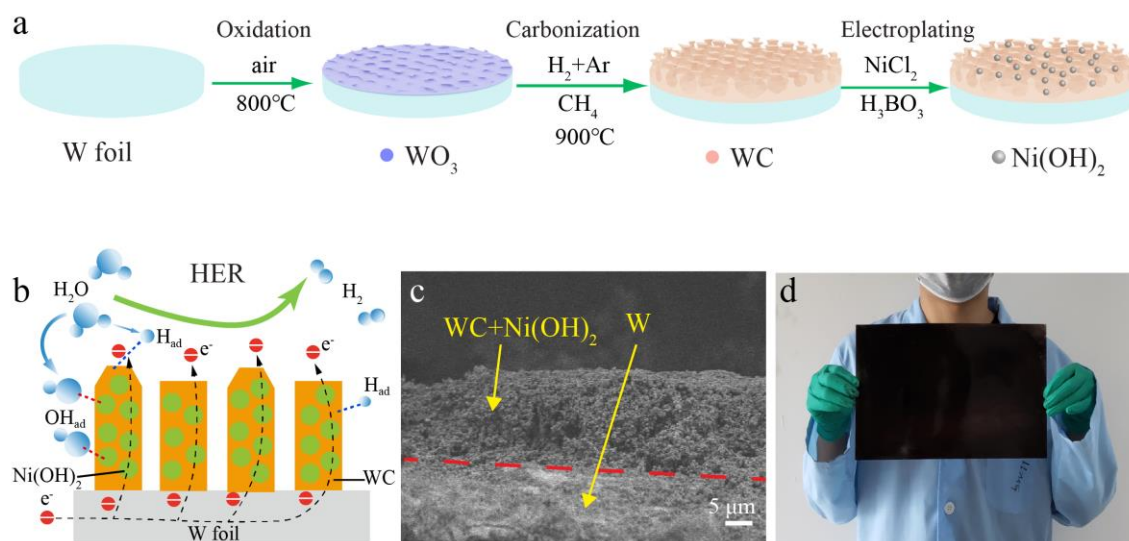
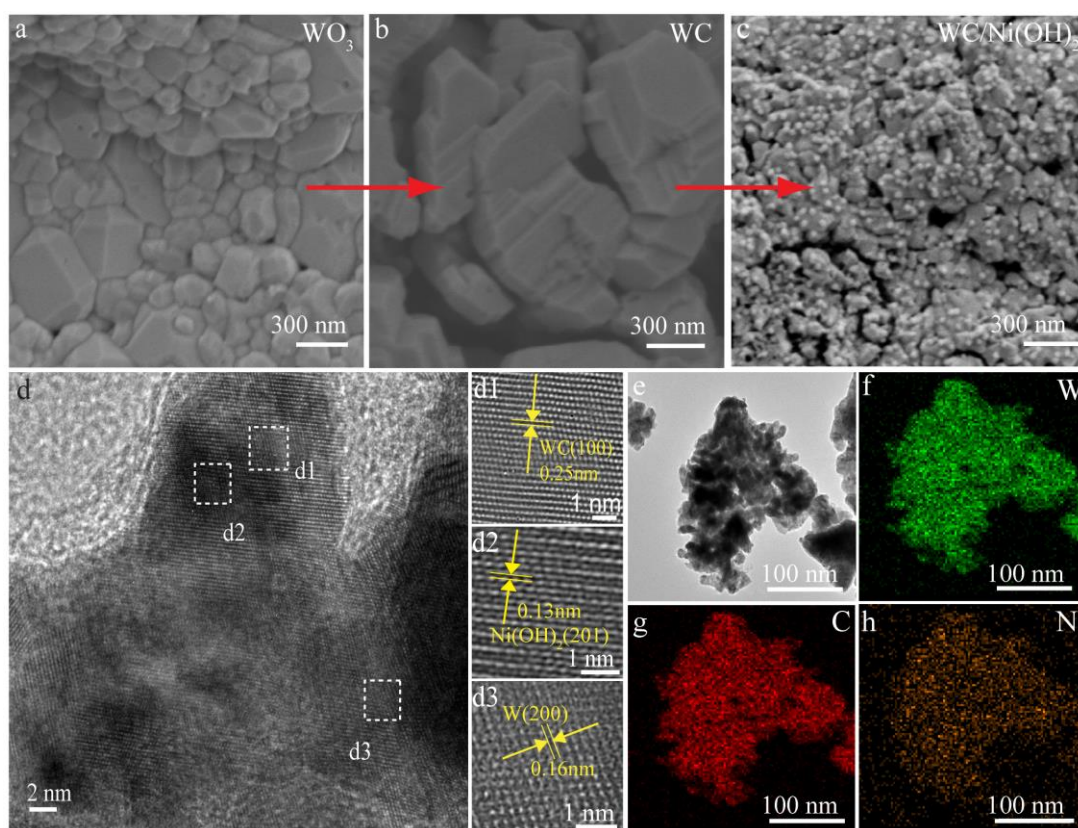


Fig. 1. (a) Illustration of the preparation process of WC/ $\text{Ni(OH)}_2$  electrodes. (b) Mechanism of HER for the WC/ $\text{Ni(OH)}_2$  catalyst in alkaline conditions. (c) Scanning electron microscopy (SEM) image of the cross-section of WC/ $\text{Ni(OH)}_2$ . (d) Optical image WC/ $\text{Ni(OH)}_2$  electrodes

As exhibited in Fig. 2a, the surface of intrinsic WO<sub>3</sub> is highly dense and smooth. After carbonization process, the complicated layered nanostructures can be observed on the surface of WC, which increases the surface area that could highly improve the performance of HER (Fig. 2b). The WC also provides abundant surface area for the electrodeposition of Ni(OH)<sub>2</sub>. After electrochemical deposition, Fig. 2c shows distinct Ni(OH)<sub>2</sub> particles on the surface of WC catalysts. The optimal deposition time of Ni(OH)<sub>2</sub> particles with 20 seconds gives moderate size and distribution compared to other deposition time.

As exhibited in Fig. 2d, the high-resolution transmission electron microscopy (HRTEM) image of WC/Ni(OH)<sub>2</sub>

indicates obvious contact between W, WC, and Ni(OH)<sub>2</sub>, which represents the multiple interfaces of W/WC/Ni(OH)<sub>2</sub>. The distance of interplane about lattice fringes can be easily measured as 0.25, 0.13, and 0.16 nm, respectively (Figs. 2d1, 2d2 and 2d3), corresponding to the hexagonal WC with the (100) crystallographic plane, hexagonal Ni(OH)<sub>2</sub> with the (201) plane, and cubic W with (200) plane, respectively. Besides, the energy-dispersive X-ray spectroscopy (EDS) elemental mapping of WC/Ni(OH)<sub>2</sub> in Fig. 2e~2h indicates that W, C, and Ni elements are distributed evenly. These results confirm the presence of the mixed phases of Ni(OH)<sub>2</sub>, WC, and W.



**Fig. 2.** (a) SEM image of synthesized WO<sub>3</sub>. (b) SEM image of carbonized WC. (c) SEM image of electrodeposited WC/Ni(OH)<sub>2</sub> with deposition time of 20 seconds. (d) HRTEM image of WC/Ni(OH)<sub>2</sub>/W. (d1-d3) Fast Fourier Transform (FTT) analysis images of WC/Ni(OH)<sub>2</sub>. (e-h) Elemental mapping of W, C, and Ni elements

Fig. 3a shows the investigation of Raman spectra. The two weak peaks at 677 and 803 cm<sup>-1</sup> can be ascribed to the stretching mode of W-C<sup>[22]</sup>. Moreover, the X-ray photoelectron spectroscopy (XPS) spectra of WC/Ni(OH)<sub>2</sub> are utilized to confirm the chemical states of W, C and Ni elements in Fig. 3b. Fig. 3c indicates that the XPS spectra of W 4f exhibit four peaks located at 37.5, 35.3, 34.2 and 32.0 eV, respectively. The last two peaks at 34.2 and 32.0 eV are

ascribed to the featured peaks of W4f<sub>7/2</sub> and W4f<sub>5/2</sub> of WC. And the peaks of W-O (37.5 and 35.3 eV) are attributed to the oxidation of the surface of WC. Ni 2p XPS spectra show four pronounced peaks located at 879.3, 873.6, 861.6 and 855.9 eV, respectively (Fig. 3d). The binding energy of 855.9 and 861.6 eV are due to Ni<sup>2+</sup>/Ni(OH)<sub>2</sub>, and the other two peaks at 873.5 and 879.3 eV result from the Ni 2p<sub>1/2</sub>, indicating the existence of Ni(OH)<sub>2</sub><sup>[23]</sup>.

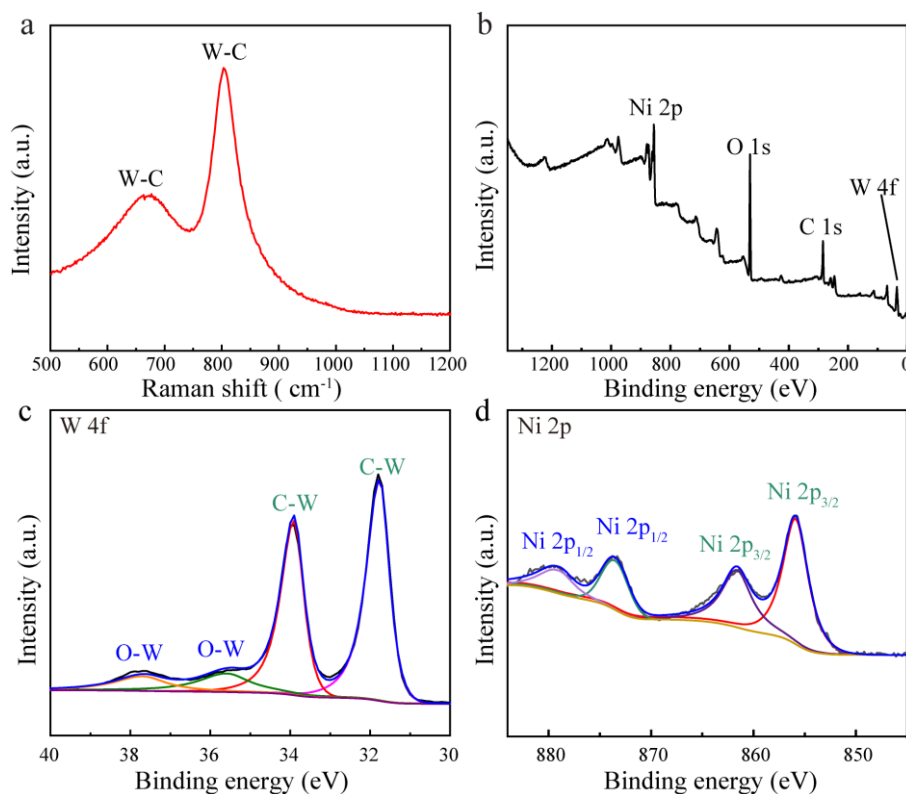


Fig. 3. (a) Raman spectra of WC foil. (b) Full XPS spectra of WC/Ni(OH)<sub>2</sub>. (c) High-resolution XPS spectra of W. (d) High-resolution XPS spectra of Ni

### 3.2 Electrocatalytic activity

All measurements about HER electrocatalytic activities of as-grown WC/Ni(OH)<sub>2</sub> material are evaluated in 1 M KOH solution via a three-electrode setup. The polarization curves are measured using linear sweep voltammetry (LSV) with a sweep rate of 5 mV/s. As exhibited in Figs. 4a and 4b, the WC/Ni(OH)<sub>2</sub> behaves as a dramatic HER activity with a low onset potential of 20 mV (vs. RHE) and an operating overpotential of 51 mV (vs. RHE) at the negative current density of 10 mA/cm<sup>2</sup> ( $\eta_{10}$ ). It is much smaller than the overpotentials of W and WC catalysts with the values of 496 mV (vs. RHE) and 109 mV (vs. RHE), respectively at the current density of 10 mA/cm<sup>2</sup>. These results demonstrate that the synergistic effect of WC/Ni(OH)<sub>2</sub> can facilitate the HER performance. Moreover, compared with 20 wt% Pt/C, Pt/C has the best activity at low overpotential (0~164 mV), while at high overpotential (> 164 mV), WC/Ni(OH)<sub>2</sub> catalyst exhibits impressively better HER performance. A maximum current density can reach 2044.0 mA/cm<sup>2</sup> at an overpotential of 800 mV (vs. RHE) for WC/Ni(OH)<sub>2</sub> catalyst, which is much higher than Pt/C.

As shown in Fig. 4c, according to the Tafel equation ( $\eta = b \log j + a$ ), the linear region of the Tafel slope is fitted. The

Tafel slope of WC/Ni(OH)<sub>2</sub> is 47.5 mV/dec, which is much smaller than that of WC and W with Tafel slopes of 99.8 and 389.6 mV/dec, respectively. 20 wt% Pt/C possesses the minimal Tafel slope with 30.6 mV/dec in 1 M KOH media. The elementary steps are related to the Tafel slope in HER. Thus, the main mechanism for WC/Ni(OH)<sub>2</sub> is the Volmer-Heyrovsky reaction whose rate-limiting step can be identified as the process of electrochemical desorption, which is different from the Volmer-Tafel mechanism for Pt/C with the rate-limiting step of combination step.

Large current density at low overpotential can not only improve the efficiency of HER but also reduce the energy consumption. Thus, Fig. 4d summarizes the HER performance for some compound catalysts compared with different reported noble metal catalysts at a large current density of 1000 mA/cm<sup>2</sup>. It can be seen that the efficiency of WC/Ni(OH)<sub>2</sub> with 475 mV (vs. RHE) at the current density of 1000 mA/cm<sup>2</sup> ( $\eta_{1000}$ ) performs better than lots of Pt catalysts and compound catalysts<sup>[14, 15, 24-27]</sup>. Moreover, the HER performance of WC becomes more efficient with increasing the concentration of alkaline solution (Fig. 4e). Especially, in a 10 M KOH solution, the current density can be as high as 3108.7 mA/cm<sup>2</sup>. Hence, the WC/Ni(OH)<sub>2</sub> hybrid structure

can be a low-cost HER candidate to replace Pt in industrial hydrogen production.

Besides, durability at high current density is also an important category for electrocatalysts. The cyclic voltammograms (CVs) with 8000 cycles are applied and the method about Amperometric *i-t* curve at the current density of 500 mA/cm<sup>2</sup> for 50 hours is also employed to test the durability of WC/Ni(OH)<sub>2</sub> (Fig. 4f). The results imply that the current

density remains stable after the *i-t* test for 50 hours. The WC/Ni(OH)<sub>2</sub> shows excellent stability in the HER durability test because of the self-supported structure. The strong bonding between W and WC makes the stability of WC/Ni(OH)<sub>2</sub> much better than the amounts of compound electrochemical catalysts. Hence, the WC/Ni(OH)<sub>2</sub> hybrid structure can be a low-cost HER candidate to replace Pt in industrial hydrogen production.

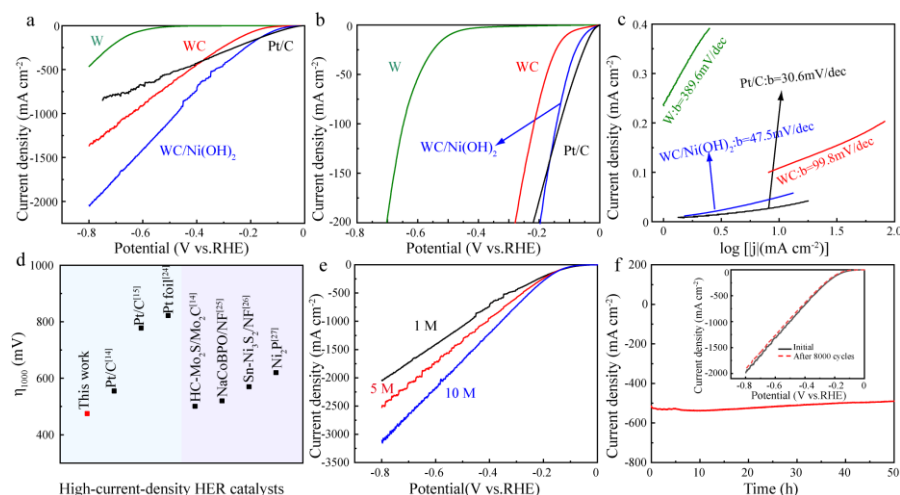


**Fig. 4.** (a) Polarization curves of WC/Ni(OH)<sub>2</sub> in 1 M KOH electrolyte at 5 mV/s, along with W foil, WC foil, and Pt/C for comparison. (b) Polarization curves of different catalysts for comparison at the current density of 200 mA/cm<sup>2</sup>. (c) Tafel plots of the catalysts shown in (a). (d) Comparison of the high-current-density of 1000 mA/cm<sup>2</sup> HER performance of the catalysts in this work with previously reported data of different catalysts. (e) Polarization curves of WC/Ni(OH)<sub>2</sub> in 1 M KOH, 5 M KOH, and 10 M KOH electrolyte at 5 mV/s, respectively. (f) Chronopotentiometry curve of WC/Ni(OH)<sub>2</sub> in 1 M KOH for 50 hours. Insert: the polarization curves of WC/Ni(OH)<sub>2</sub> initially and 8000 cycles in 1 M KOH at a scan rate of 5 mV/s

## 4 CONCLUSION

In summary, we have developed a high current density, efficient, and stable WC/Ni(OH)<sub>2</sub> nanostructures seamlessly grown on W foils by a convenient annealing method. The seamless contact between different composites improves the efficiency of charge transfer. The adsorption of hydrogen of WC is neither strong nor weak and Ni(OH)<sub>2</sub> can dissociate

water and adsorb OH<sub>ad</sub> effectively. The seamless contact and the synergy of WC and Ni(OH)<sub>2</sub> highly enhance the HER performance. The as-prepared WC/Ni(OH)<sub>2</sub> displays a small Tafel slope of 47.5 mV/dec, 475 mV (vs. RHE) at 1000 mA/cm<sup>2</sup> current density and long-term stability of 50 hours after the *i-t* test for 50 hours. We offer a route for a stable HER electrocatalyst with high current density on large scale for the industrial manufacturing by a simple thermal process.

## REFERENCES

- (1) Voiry, D.; Shin, H. S.; Loh, K. P.; Chhowalla, M. Low-dimensional catalysts for hydrogen evolution and CO<sub>2</sub> reduction. *Nat. Rev. Chem.* **2018**, 2, 1–17.
- (2) Xie, J.; Li, S.; Zhang, X.; Zhang, J.; Wang, R.; Zhang, H.; Pan, B.; Xie, Y. Atomically-thin molybdenum nitride nanosheets with exposed active surface sites for efficient hydrogen evolution. *Chem. Sci.* **2014**, 5, 4615–4620.
- (3) Jian, C.; Cai, Q.; Hong, W.; Li, J.; Liu, W. Edge-riched MoSe<sub>2</sub>/MoO<sub>2</sub> hybrid electrocatalyst for efficient hydrogen evolution reaction. *Small* **2018**, 14, e1703798–7.
- (4) Nong, S.; Dong, W.; Yin, J.; Dong, B.; Lu, Y.; Yuan, X.; Wang, X.; Bu, K.; Chen, M.; Jiang, S.; Liu, L. M.; Sui, M.; Huang, F. Well-dispersed ruthenium in mesoporous crystal TiO<sub>2</sub> as an advanced electrocatalyst for hydrogen evolution reaction. *J. Am. Chem. Soc.* **2018**, 140, 5719–5727.
- (5) Zou, X.; Zhang, Y. Noble metal-free hydrogen evolution catalysts for water splitting. *Chem. Soc. Rev.* **2015**, 44, 5148–5180.

- (6) Chung, D. Y.; Jun, S. W.; Yoon, G.; Kim, H.; Yoo, J. M.; Lee, K. S.; Kim, T.; Shin, H.; Sinha, A. K.; Kwon, S. G.; Kang, K.; Hyeon, T.; Sung, Y. E. Large-scale synthesis of carbon-shell-coated FeP nanoparticles for robust hydrogen evolution reaction electrocatalyst. *J. Am. Chem. Soc.* **2017**, 139, 6669–6674.
- (7) Shi, Y.; Zhou, Y.; Yang, D. R.; Xu, W. X.; Wang, C.; Wang, F. B.; Xu, J. J.; Xia, X. H.; Chen, H. Y. Energy level engineering of MoS<sub>2</sub> by transition-metal doping for accelerating hydrogen evolution reaction. *J. Am. Chem. Soc.* **2017**, 139, 15479–15485.
- (8) Han, N.; Yang, K. R.; Lu, Z.; Li, Y.; Xu, W.; Gao, T.; Cai, Z.; Zhang, Y.; Batista, V. S.; Liu, W.; Sun, X. Nitrogen-doped tungsten carbide nanoarray as an efficient bifunctional electrocatalyst for water splitting in acid. *Nat. Commun.* **2018**, 9, 924–10.
- (9) Wang, P.; Zhang, X.; Zhang, J.; Wan, S.; Guo, S.; Lu, G.; Yao, J.; Huang, X. Precise tuning in platinum-nickel/nickel sulfide interface nanowires for synergistic hydrogen evolution catalysis. *Nat. Commun.* **2017**, 8, 14580–9.
- (10) Zhang, Z. C.; Xu, B.; Wang, X. Engineering nanointerfaces for nanocatalysis. *Chem. Soc. Rev.* **2014**, 43, 7870–7886.
- (11) Yamada, Y.; Tsung, C. K.; Huang, W.; Huo, Z.; Habas, S. E.; Soejima, T.; Aliaga, C. E.; Somorjai, G. A.; Yang, P. Nanocrystal bilayer for tandem catalysis. *Nat. Chem.* **2011**, 5, 372–376.
- (12) Ma, L.; Hu, Y.; Zhu, G.; Chen, R.; Chen, T.; Lu, H.; Wang, Y.; Liang, J.; Liu, H.; Yan, C.; Tie, Z.; Jin, Z.; Liu, J. *In situ* thermal synthesis of inlaid ultrathin MoS<sub>2</sub>/graphene nanosheets as electrocatalysts for the hydrogen evolution reaction. *Chem. Mater.* **2016**, 28, 5733–5742.
- (13) Shi, M.; Li, W.; Fang, J.; Jiang, Z.; Gao, J.; Chen, Z.; Sun, F.; Xu, Y. Electronic structure tuning during facile construction of two-phase tungsten based electrocatalyst for hydrogen evolution reaction. *Electrochim. Acta* **2018**, 283, 834–841.
- (14) Zhang, C.; Luo, Y.; Tan, J.; Yu, Q.; Yang, F.; Zhang, Z.; Yang, L.; Cheng, H. M.; Liu, B. High-throughput production of cheap mineral-based two-dimensional electrocatalysts for high-current-density hydrogen evolution. *Nat. Commun.* **2020**, 11, 3724–8.
- (15) Chen, Y.; Yu, G.; Chen, W.; Liu, Y.; Li, G. D.; Zhu, P.; Tao, Q.; Li, Q.; Liu, J.; Shen, X.; Li, H.; Huang, X.; Wang, D.; Asefa, T.; Zou, X. Highly active, nonprecious electrocatalyst comprising borophene subunits for the hydrogen evolution reaction. *J. Am. Chem. Soc.* **2017**, 139, 12370–12373.
- (16) Li, J.; Hong, W.; Jian, C.; Cai, Q.; He, X.; Liu, W. High-performance hydrogen evolution at a MoSe<sub>2</sub>-Mo<sub>2</sub>C seamless heterojunction enabled by efficient charge transfer. *J. Mater. Chem. A* **2020**, 8, 6692–6698.
- (17) Ma, Y. Y.; Lang, Z. L.; Yan, L. K.; Wang, Y. H.; Tan, H. Q.; Feng, K.; Xia, Y. J.; Zhong, J.; Liu, Y.; Kang, Z. H.; Li, Y. G. Highly efficient hydrogen evolution triggered by a multi-interfacial Ni/WC hybrid electrocatalyst. *Energy Environ. Sci.* **2018**, 11, 2114–2123.
- (18) Yang, C.; Zhao, R.; Xiang, H.; Wu, J.; Zhong, W.; Li, W.; Zhang, Q.; Yang, N.; Li, X. Ni-activated transition metal carbides for efficient hydrogen evolution in acidic and alkaline solutions. *Adv. Energy Mater.* **2020**, 10, 2002260–10.
- (19) Danilovic, N.; Subbaraman, R.; Strmcnik, D.; Chang, K. C.; Paulikas, A. P.; Stamenkovic, V. R.; Markovic, N. M. Enhancing the alkaline hydrogen evolution reaction activity through the bifunctionality of Ni(OH)<sub>2</sub>/metal catalysts. *Angew. Chem., Int. Ed.* **2012**, 51, 12495–12498.
- (20) Subbaraman, R.; Tripkovic, D.; Chang, K. C.; Strmcnik, D.; Paulikas, A. P.; Hirunsit, P.; Chan, M.; Greeley, J.; Stamenkovic, V.; Markovic, N. M. Trends in activity for the water electrolyser reactions on 3d M (Ni, Co, Fe, Mn) hydr(oxy)oxide catalysts. *Nat. Mater.* **2012**, 11, 550–557.
- (21) Loget, G.; Fabre, B.; Fryars, S.; Méridac, C.; Ababou-Girard, S. Dispersed Ni nanoparticles stabilize silicon photoanodes for efficient and inexpensive sunlight-assisted water oxidation. *ACS Energy Lett.* **2017**, 2, 569–573.
- (22) Zhang, L. N.; Ma, Y. Y.; Lang, Z. L.; Wang, Y. H.; Khan, S. U.; Yan, G.; Tan, H. Q.; Zang, H. Y.; Li, Y. G. Ultrafine cable-like WC/W<sub>2</sub>C heterojunction nanowires covered by graphitic carbon towards highly efficient electrocatalytic hydrogen evolution. *J. Mater. Chem. A* **2018**, 6, 15395–15403.
- (23) Li, C.; Wang, J.; Wang, Y.; Li, J.; Yao, Z.; Jiang, Z. Enhancing hydrogen evolution reaction by synergistically coupling NiMo alloy with Ni(OH)<sub>2</sub> nanosheet on carbon cloth. *ChemistrySelect* **2020**, 5, 6774–6779.
- (24) Luo, Y.; Tang, L.; Khan, U.; Yu, Q.; Cheng, H. M.; Zou, X.; Liu, B. Morphology and surface chemistry engineering toward pH-universal catalysts for hydrogen evolution at high current density. *Nat. Commun.* **2019**, 10, 269–7.
- (25) Menezes, P. W.; Indra, A.; Zaharieva, I.; Walter, C.; Loos, S.; Hoffmann, S.; Schlögl, R.; Dau, H.; Driess, M. Helical cobalt borophosphates to master durable overall water-splitting. *Energy Environ. Sci.* **2019**, 12, 988–999.
- (26) Jian, J.; Yuan, L.; Qi, H.; Sun, X.; Zhang, L.; Li, H.; Yuan, H.; Feng, S. Sn-Ni<sub>3</sub>S<sub>2</sub> ultrathin nanosheets as efficient bifunctional water-splitting catalysts with a large current density and low overpotential. *ACS Appl. Mater. Interfaces* **2018**, 10, 40568–40576.
- (27) Yu, L.; Mishra, I. K.; Xie, Y.; Zhou, H.; Sun, J.; Zhou, J.; Ni, Y.; Luo, D.; Yu, F.; Yu, Y.; Chen, S.; Ren, Z. Ternary Ni<sub>2(1-x)</sub>Mo<sub>2x</sub>P nanowire arrays toward efficient and stable hydrogen evolution electrocatalysis under large-current-density. *Nano Energy* **2018**, 53, 492–500.